Article:
Cheshire, D. M., Backes, D., Veiga, L. S.I. et al. (2025) Increased Gilbert damping in yttrium iron garnet by low temperature vacuum annealing. Applied Physics Letters. 112405. ISSN: 0003-6951

https://doi.org/10.1063/5.0244429

Applied Physics Letters

RESEARCH ARTICLE | MARCH 19 2025

Increased Gilbert damping in yttrium iron garnet by low temperature vacuum annealing

D. M. Cheshire ; D. Backes ; L. S. I. Veiga ; S. S. Dhesi ; S. A. Cavill

Appl. Phys. Lett. 126, 112405 (2025)
https://doi.org/10.1063/5.0244429

Increased Gilbert damping in yttrium iron garnet by low temperature vacuum annealing

Cite as: Appl. Phys. Lett. **126**, 112405 (2025); doi: 10.1063/5.0244429
Submitted: 18 October 2024 · Accepted: 6 March 2025 ·
Published Online: 19 March 2025

D. M. Cheshire,[1] D. Backes,[2] L. S. I. Veiga,[2] S. S. Dhesi,[2] and S. A. Cavill[1,a)]

AFFILIATIONS

[1]School of Physics, Engineering and Technology, University of York, York YO10 5DD, United Kingdom
[2]Diamond Light Source, Harwell Science and Innovation Campus, Chilton, Didcot OX11 ODE, United Kingdom

[a)]Author to whom correspondence should be addressed: stuart.cavill@york.ac.uk

ABSTRACT

The effect of thermal surface cleaning on the Gilbert damping (α) of yttrium iron garnet (YIG), before capping with a metallic layer, has been investigated. Our results show that α is strongly affected by relatively mild annealing conditions ($T = 300\,^{\circ}\mathrm{C}$) when performed in a vacuum. This increase needs to be taken into account when obtaining the spin-mixing conductance from spin pumping measurements. We measure an increase in α by a factor of $\times 8$ when the YIG is vacuum annealed at 300 °C. No such changes in α are observed when annealed at the same temperature in 1×10^{-1} mbar of oxygen. We suggest that the main driver for the increase in α is the reduction of Fe^{3+} to Fe^{2+}, as demonstrated by soft x-ray magnetic spectroscopy.

Research in the sub-field of magnon spintronics, where magnons—the quanta of spin waves—are used to carry and process information, has gathered pace in recent years.[1–3] Magnons offer several advantages over conventional spintronics, particularly in the development of insulator-based devices with reduced energy consumption. In these devices, the propagation of pure spin currents in magnetic insulators, where dissipationless transport of the spin has been predicted,[4] eliminates parasitic Joule heating. One magnetic insulator in particular, yttrium iron garnet (YIG), is considered the most prominent material in this field, being widely used in spin transport experiments[5] due to its exceptionally low damping, even in thin films.[6] In order to combine magnon spintronics and charge-based electronics, the latter crucial for input–output functionality, it is necessary to create efficient converters that transform magnon spin currents into conventional charge currents. Typically, spin pumping, which generates spin accumulation in a metal by magnetization precession of an adjacent ferromagnet, and the inverse spin Hall effect (ISHE), which transforms a pure spin current into a charge current, are used for the input and output conversion processes, respectively. According to the spin pumping theory,[7] the spin current sunk by a layer adjacent to a ferromagnet (FM) leads to an increase in the Gilbert damping such that $\alpha = \alpha_{intrinsic} + \alpha_{sp}$, with

$$\alpha_{sp} = \frac{g\mu_B}{4\pi M_s} g_{eff}^{\uparrow\downarrow} \frac{1}{d}, \tag{1}$$

where M_s is the saturation magnetization of the FM, d is the FM layer thickness, g is the spectroscopic g-factor, and $g_{eff}^{\uparrow\downarrow}$ is the effective spin-mixing conductance that essentially governs the transfer of spin momentum across an interface. Measuring the change in the Gilbert damping of the YIG due to spin pumping (α_{sp}) into an adjacent metallic layer therefore allows a convenient experimental determination of $g_{eff}^{\uparrow\downarrow}$.[7–9]

Previous studies on spin-mixing conductance at a YIG/Pt interface demonstrated an enhancement by more than two orders of magnitude by surface treatments, such as Piranha etch and heating the sample at 500 °C in vacuum, prior to Pt deposition.[10] The authors considered that the intrinsic Gilbert damping is the same for all samples, irrespective of treatment method, so that changes in damping are solely related to changes in $g_{eff}^{\uparrow\downarrow}$.

In this paper, we report increases in the Gilbert damping in YIG thin films, due to either being subjected to vacuum thermal annealing, or the subsequent deposition of a thin (2 nm) weak spin–orbit coupled aluminum capping layer. The Gilbert damping is observed to increase significantly for YIG, vacuum annealed at 300 °C for as little as 15 minutes, whereas for YIG annealed at the same temperature in a 1×10^{-1} mbar partial pressure of oxygen, α is unaffected. In addition, we notice that the deposition of Al on the YIG, irrespective of film heat treatment, also increases α. We argue that such increases need to be considered when forming spin pumping heterostructures as often the YIG films are annealed in vacuum to remove physisorbed gas species

(air, water vapor) from the surface prior to heavy metal deposition. These increases in α may then be incorrectly attributed to α_{sp}, leading to errors in $g_{eff}^{\uparrow\downarrow}$. We suggest that the main driver for the increase in α is the reduction of Fe^{3+} to Fe^{2+}, consistent with vacuum annealing and/or a displacement reaction between Fe oxide and Al. Changes in the Fe $L_{2,3}$ x-ray absorption spectra, with annealing conditions and capping layer material, support this hypothesis.

Crystalline YIG films were grown via pulsed laser deposition (PLD) on (111)-oriented gadolinium gallium garnet (GGG) substrates. Following Refs. 11 and 12 an amorphous YIG layer was deposited at room temperature, in a partial oxygen pressure of 2.5×10^{-3} mbar, by ablating a stoichiometric polycrystalline YIG target. Ablation was performed using a frequency quadrupled Nd:YAG laser ($\lambda = 266$ nm) with a fluence of approximately 1 J cm^{-2}, at a repetition frequency of 10 Hz. The sample was rotated at 6 RPM during deposition. Following deposition, the amorphous YIG samples were *ex situ* annealed in atmospheric conditions, at 850 °C for 3 h, to recrystallize the YIG. This technique was used to produce four YIG films with nominal thicknesses of (65 ± 3) nm for FMR measurements.

Post FMR, the four epitaxial single crystal YIG films were subjected to surface treatments, as summarized in Table I. Two films, (b) and (d), were annealed in vacuum (base pressure of 5×10^{-8} mbar), using *in situ* laser heating in the PLD chamber. Film (b) was annealed at 150 °C, while film (d) was annealed at 300 °C: both for 15 min. The temperature was ramped at approximately 4 °C/min by adjusting the duty cycle of a pulsed 10.6 μm CO_2 laser directed onto the back of the samples. The third film, (c), was annealed at 300 °C under an oxygen partial pressure of 1×10^{-1} mbar, following the same procedure. The fourth film (a) was annealed at 150 °C under the same oxygen partial pressure, and served as a control. FMR measurements were then repeated on the treated films to observe changes to the magnetic damping. These thermal annealing treatments were repeated on two additional sets of recrystallized YIG films to ensure repeatability.

To facilitate total electron yield (TEY) detection for x-ray absorption spectroscopy (XAS)/x-ray magnetic circular dichroism (XMCD) spectroscopy measurements, an additional 2 nm aluminum capping layer was then deposited on three of the treated YIG films (b–d) by sputtering a pure Al target at room temperature. The fourth YIG film (a), used as a control, was capped with a 2 nm platinum capping layer deposited at room-temperature using PLD, ablating a pure Pt target in vacuum (base pressure of 5×10^{-8} mbar). A final set of FMR measurements was performed on the four capped YIG films, prior to XAS/XMCD measurement.

The Gilbert damping of the YIG was measured using in-plane FMR spectroscopy by mounting the samples face down onto a 50 Ω coplanar waveguide (CPW), connected to a two-port vector network analyzer (VNA) and centered between the poles of a 2D vector magnet. Details of the system can be found in Ref. 13. The microwave transmission S-wave parameter, S_{12}, was measured over a frequency range of 0.001–15 GHz. The applied magnetic field ranged from 0 to 4 kOe, with a field step of 0.2 Oe, producing a 2D frequency-field resonance map, as shown in Fig. S1 of the supplementary material. All FMR measurements were performed at an RF power of +7 dBm. Field linescans at constant frequency were extracted from the FMR frequency-field maps and fitted using an asymmetric Lorentzian function[14,15] to determine the corresponding resonance field (H_r) and linewidth (ΔH), see Fig. S1. Fe $L_{2,3}$ XAS and XMCD measurements were performed on beamline I06 at the Diamond Light Source.[16] The XAS was measured in normal incidence, which reduces the effect of self-absorption on the spectra,[17] in a 6 T field applied collinear to the x-ray helicity vector by total electron yield (TEY). At the $L_{2,3}$ absorption edges of 3d transition metals, the probing depth for TEY detection is approximately 6 nm.

TABLE I. Summary of annealed YIG/GGG thin film samples, with 2 nm metallic capping layers.

YIG sample	*In situ* annealing (15 min)	Capping layer
(a)	150 °C, Oxygen (1×10^{-1} mbar)	Pt
(b)	150 °C, Vacuum (5×10^{-8} mbar)	Al
(c)	300 °C, Oxygen (1×10^{-1} mbar)	Al
(d)	300 °C, Vacuum (5×10^{-8} mbar)	Al

Resonant frequencies were extracted from the frequency-field maps for each applied field and are plotted in Fig. 1 for the YIG films prepared under different conditions. We also include an additional sample,[18] annealed at 300 °C in O_2 and capped with 2 nm of Pt for completeness. The FMR resonance frequency as a function of field is fit to the easy-axis in-plane Kittel equation for a (111) orientated film, given by

$$\omega = \gamma\sqrt{(H(H + 4\pi M_{eff}))}, \tag{2}$$

with the gyromagnetic ratio $\gamma = g\mu_B/\hbar$, and the effective magnetization $M_{eff} = 4\pi M_s - K/M_s$, where M_s is the saturation magnetization of the YIG, and K is the cubic magnetocrystalline anisotropy constant (−6100 erg/cc for YIG).[19] For three of the YIG films (a–c), the FMR resonant field (measured at 10 GHz) of all three stages differ by less than 8 Oe, with the Kittel curves almost lying on top of each other. The variation in the Kittel curves are so small that they display as a single overlapping curve, i.e., the parameters such as the saturation magnetization (M_s), the anisotropy (K), and gyromagnetic ratio (γ) are the same within error, leading to Kittel curves that are almost overlapping. A zoomed in version of Fig. 1 at 10 GHz is shown in the supplementary material, Fig. S2. However, for YIG vacuum annealed at 300 °C [Fig. 1(d)], a more significant decrease in resonant field (H_r) of 95 Oe is observed, with an additional decrease in 18 Oe following aluminum capping. Nevertheless, Kittel curve fits for all four films produce values for M_s that agree within error with independent measurements of the films using vibrating sample magnetometry, (131 ± 6) emu/cc. The three films with similar Kittel curves also produce a similar g-factor of (2.02 ± 0.01) across all processing stages of these three samples, close to the expected value of 2 for a d^5 ion.[20–22] However, the 300 °C vacuum-annealed YIG film produces a larger g-factor of (2.050 ± 0.005).

In samples where two-magnon scattering is negligible, the magnetic linewidth (Δ H) of the FMR resonance follows a linear dependence with microwave frequency, such that[23,24]

$$\Delta H(f) = \Delta H_0 + \frac{2\pi\alpha f}{\gamma}, \tag{3}$$

where ΔH is the half width at half maximum (HWHM) of the resonance, α is the intrinsic Gilbert damping, γ is the gyromagnetic ratio,

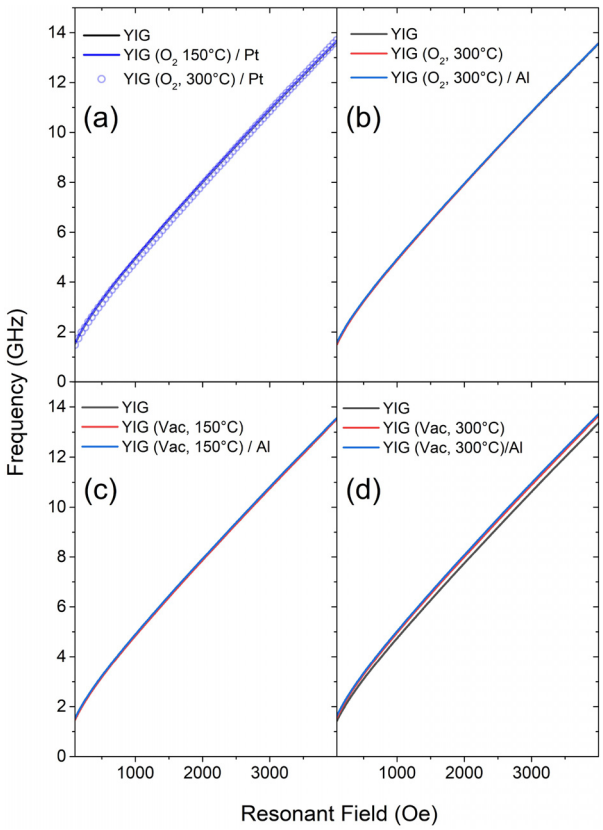

FIG. 1. Kittel curves (frequency vs field) for the (black) as-grown, (red) annealed YIG films, and (blue) annealed YIG films after capping with 2 nm metal layer. (a) YIG/Pt, (b) YIG (vac, 150 °C)/Al, (c) YIG (O_2, 300 °C)/Al, and (d) YIG (vac, 300 °C)/Al samples. The open circles in (a) are from an additional YIG/Pt sample annealed at 300 °C in O_2: We note that only 1 in 50 of the data points are plotted for clarity.

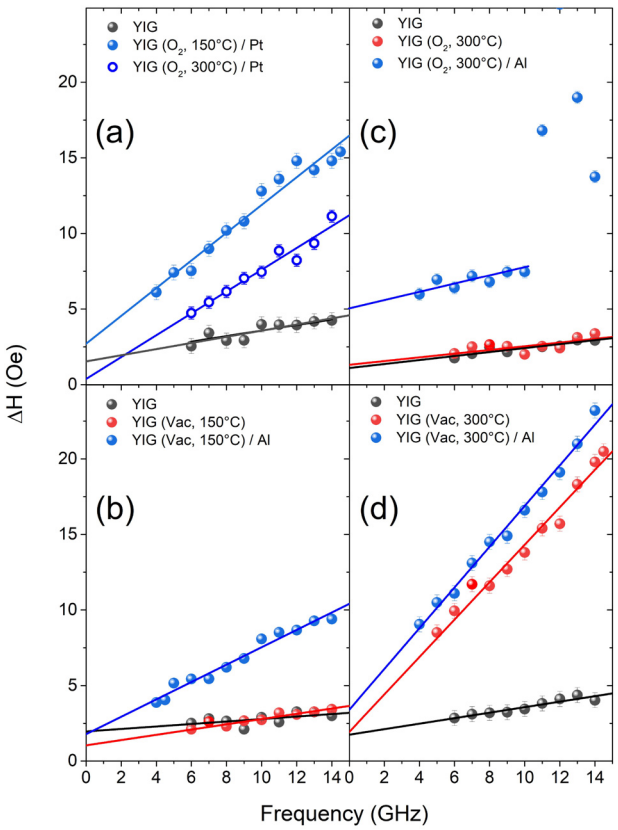

FIG. 2. FMR linewidth (Δ H) vs frequency for the (black) as-grown, (red) annealed YIG films, and (blue) annealed YIG films after capping with 2 nm metal layer. (a) YIG/Pt, (b) YIG (vac, 150 °C)/Al, (c) YIG (O_2, 300 °C)/Al, and (d) YIG (vac, 300 °C)/Al samples. The open circles in (a) are from an additional YIG/Pt sample annealed at 300 °C in O_2 for completeness.

and ΔH_0 is the frequency independent extrinsic damping. The experimental data for magnetic linewidth as a function of microwave frequency are shown in Fig. 2.

Fitting Eq. (3) to the data in Fig. 2 allows for the extraction of the Gilbert damping (α) and frequency independent extrinsic damping (ΔH_0) for each of the treated YIG conditions. ΔH vs f is linear for all samples (prior to Al deposition), indicating that two-magnon scattering is not significant in our samples, even those annealed in vacuum. We observe no significant increases in the Gilbert damping that arise from in-vacuum annealing of the YIG at 150 °C [Fig. 2(b)]. However, in-vacuum annealing at 300 °C [Fig. 2(d)]—even for only 15 min—dramatically increases the Gilbert damping, by almost an order of magnitude upon re-measurement of the FMR: from $(5.0 \pm 0.6)\times10^{-4}$ to $(38 \pm 1)\times10^{-4}$. In contrast, for annealing performed at 300 °C in 1×10^{-1} mbar of pure oxygen [Fig. 2(c)], the Gilbert damping was found to be, within error, unchanged. This is an important observation and highlights the sensitivity of YIG FMR to preparation conditions, such as thermal cleaning of physisorbed species, that may be used when depositing multiple layers for magnonic devices. No obvious relationship between annealing treatment and extrinsic damping was inferred from the FMR data, prior to deposition of the capping layer.

In all three annealing treatments, the changes in extrinsic damping are either within error, or insignificantly small, with ΔH_0 of (1.5 ± 0.5) Oe for all cases, see Table II. This suggests that the annealing temperatures used, despite being high enough to affect the Gilbert damping when performed in vacuum, does not significantly promote the formation of defects in the bulk of the YIG film.

Interestingly, the addition of an aluminum layer causes a notable increase in Gilbert damping for all the YIG films. At first consideration, this is not expected as aluminum ($Z = 13$) is non-magnetic with a weak spin–orbit coupling and therefore would not be a natural choice for a spin-sink. The low layer thickness (2 nm) and natural oxidation, after removal from the sputtering chamber, precludes significant eddy current damping as the cause. In addition, we rule out radiative damping[25,26] as significant, as we obtain $\alpha^{rad} = 2\times10^{-5}$ from Eq. (6) in Ref. 26 for our geometry. However, an unexpected second FMR resonance mode was observed in the oxygen-annealed YIG film following aluminum deposition, see Fig. S3 in the supplementary material. The presence of this second mode restricted the frequency range across which the HWHM linewidths of the Kittel mode could be accurately determined to below 10 GHz as reflected in Fig. 2(c), as above this frequency, the two modes significantly overlapped

TABLE II. Values of Gilbert (α) and extrinsic (ΔH_0) damping of annealed YIG/GGG thin film samples, with 2 nm metallic capping layers, extracted from Fig. 2.

Sample/treatment		α ($\times 10^{-4}$)	ΔH_0 (Oe)
(a)	YIG	(5.2 ± 0.7)	(1.8 ± 0.2)
	YIG (O_2, 150 °C)/Pt	(20 ± 2)	(2.7 ± 0.6)
	YIG (O_2, 300 °C)/Pt	(26 ± 2)	(0.4 ± 0.6)
(b)	YIG	(2 ± 1)	(2.0 ± 0.4)
	YIG (Vac, 150 °C)	(4.9 ± 0.5)	(1.0 ± 0.2)
	YIG (Vac, 150 °C)/Al	(16.1 ± 0.9)	(1.8 ± 0.3)
(c)	YIG	(3.7 ± 0.6)	(1.1 ± 0.2)
	YIG (O_2, 300 °C)	(3 ± 1)	(1.3 ± 0.5)
	YIG (O_2, 300 °C)/Al	(6 ± 2)	(5.1 ± 0.5)
(d)	YIG	(5.0 ± 0.6)	(1.8 ± 0.2)
	YIG (Vac, 300 °C)	(36 ± 2)	(1.9 ± 0.7)
	YIG (Vac, 300 °C)/Al	(38 ± 1)	(3.4 ± 0.5)

broadening the resonance. The cause of this second resonance is not clear, but we speculate that it may be due to an inhomogeneous Al layer or a slight increase in the roughness of the YIG film at the YIG/Al interface, induced by the sputtering process. However, it is clear from the slope of ΔH vs frequency and values of the Gilbert damping that there is little change in α after annealing at 300 °C in oxygen prior to deposition of the capping layer.

To gain a detailed understanding of the annealed YIG, XAS/XMCD measurements were performed at the Fe $L_{2,3}$ absorption edges in order to determine the valency, coordination, and magnetic properties of the Fe cations. In L-edge XAS, electrons are excited from a 2p core level to the unoccupied 3d valence states of the element of interest by circularly polarized x-rays at the resonance energy of the transition. The difference in absorption for opposite chirality (σ_+, σ_-) of the polarizations (XMCD) gives a direct and element-specific measurement of the projection of the 3d magnetic moment along the x-ray helicity vector.[27] Due to the optical selection rules, the electric-dipole transitions from the ground state can reach only a limited subset of final states. It therefore results in a local probe with a high sensitivity to the crystal field, spin–orbit interaction, oxidation state, and site symmetry as evidenced by spectral shifts of the absorption peaks.

Figure 3 shows XAS data for the (a) YIG/Pt, (b) YIG (vac, 150 °C)/Al, (c) YIG (O_2, 300 °C)/Al, and (d) YIG (vac, 300 °C)/Al samples at the Fe $L_{2,3}$ edges. The XAS shows multiplet structure typical of YIG. Two main peaks, one negative and one positive, are present in the XMCD spectra at the L_3 edge, identical to that found in other XMCD studies of YIG.[20,28–30] These peaks correspond to contributions from Fe^{3+} in octahedral (O_h) and Fe^{3+} in tetrahedral (T_d) sites. For the ferrimagnetic garnet structure, spins located on the T_d sites are aligned antiparallel to the spins on the O_h sites in a ratio of 3:2. Hence, the negative peak in the XMCD at the L_3 edge is due to tetrahedrally coordinated Fe^{3+}. However, on annealing in an increasingly reducing environment, we notice a change in both the XAS and XMCD close to the pre-edge region of both the L_3 and L_2 edges, as shown in the gray boxed regions of Figs. 3 and 4. This change is subtle for the low temperature vacuum annealed film and 300 °C O_2 film but significant for

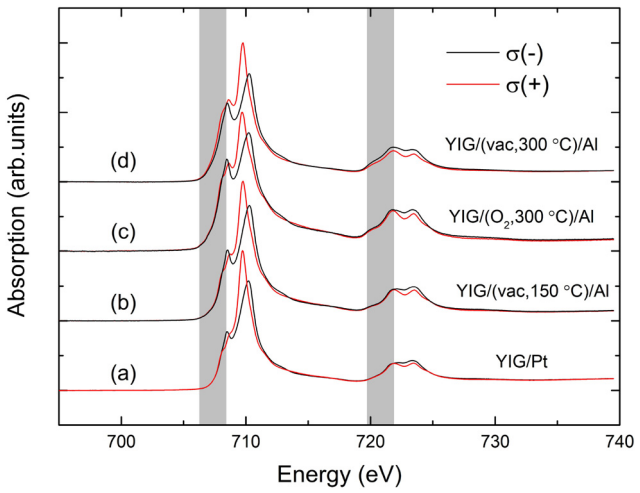

FIG. 3. Circular polarization-dependent XAS at the Fe $L_{2,3}$ edges for the (a) YIG/Pt, (b) YIG (vac, 150 °C)/Al, (c) YIG (O_2, 300 °C)/Al, and (d) YIG (vac, 300 °C)/Al samples. Pre-edge regions of the $L_{2,3}$ edges shown in gray. The spectra have been offset for clarity.

the 300 °C vacuum annealed film. The clear increase in spectral weight that occurs toward lower photon energies is indicative of an increase in Fe^{2+}, similar to the XMCD of a mixed valence Fe oxide containing Fe^{2+} and Fe^{3+}, such as Fe_3O_4,[15] that shows the relative energies of the Fe ions in different valence states around the Fe L_3 edge. The increased spectra weight at lower energies, in both XAS and XMCD data, is consistent with annealing in a reducing vacuum environment and/or a displacement reaction between iron oxide and metallic aluminum. To further demonstrate this, we integrate the XMCD in the pre-edge region of the L_3 edge (gray box). For the Pt capped sample, the integral is slightly positive, shown in Fig. 4, but becomes increasingly negative as the samples are progressively reduced. This indicates an increasing

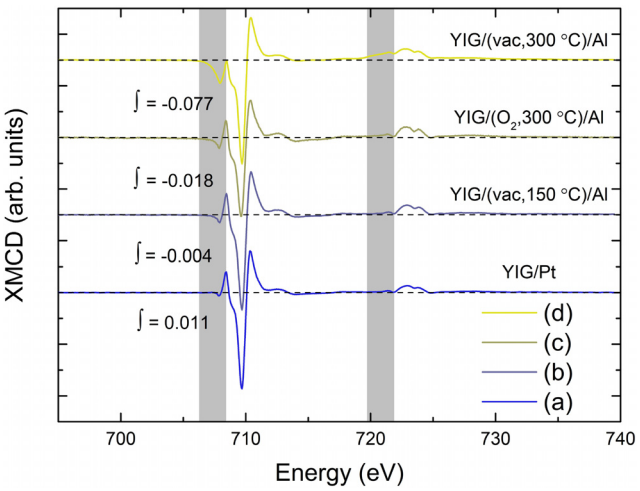

FIG. 4. XMCD spectra at the Fe $L_{2,3}$ edges for (a) YIG/Pt, (b) YIG (vac, 150 °C)/Al, (c) YIG (O_2, 300 °C)/Al, and (d) YIG (vac, 300 °C)/Al samples. Pre-edge regions of the $L_{2,3}$ edges shown in gray. The spectra have been offset for clarity.

amount of Fe^{2+}, aligned parallel to the T_d Fe^{3+} in the near surface region. As Fe^{2+} has a larger orbital moment compared to Fe^{3+}, any increase in the former would provide an additional relaxation mechanism to the lattice,[31–33] thereby enhancing the Gilbert damping, consistent with the FMR results.

In conclusion, we demonstrate that moderate vacuum annealing of YIG or the addition of an aluminum capping layer significantly increases the Gilbert damping. For the former case, this increase needs to be taken into account when obtaining the spin-mixing conductance from spin pumping measurements. We suggest that the main driver for the increase in α is the reduction of Fe^{3+} to Fe^{2+}, as demonstrated by soft x-ray magnetic spectroscopy.

See the supplementary material for further details of the FMR analysis.

The authors acknowledge Diamond Light Source for time on Beamline I06 under Proposal No. MM32492.

AUTHOR DECLARATIONS

Conflict of Interest

The authors have no conflicts to disclose.

Author Contributions

D. M. Cheshire: Formal analysis (equal); Investigation (lead); Writing – review & editing (equal). **D. Backes:** Investigation (supporting); Writing – review & editing (equal). **L. S. I. Veiga:** Investigation (supporting); Writing – review & editing (equal). **S. S. Dhesi:** Investigation (supporting); Writing – review & editing (equal). **S. A. Cavill:** Conceptualization (lead); Formal analysis (equal); Investigation (supporting); Supervision (lead); Writing – original draft (lead); Writing – review & editing (equal).

DATA AVAILABILITY

The data that support the findings of this study are available from the corresponding author upon reasonable request.

REFERENCES

[1]A. V. Chumak, P. Kabos, M. Wu, C. Abert, C. Adelmann, A. O. Adeyeye, J. Akerman, F. G. Aliev, A. Anane, A. Awad, C. H. Back, A. Barman, G. E. W. Bauer, M. Becherer, E. N. Beginin, V. A. S. V. Bittencourt, Y. M. Blanter, P. Bortolotti, I. Boventer, D. A. Bozhko, S. A. Bunyaev, J. J. Carmiggelt, R. R. Cheenikundil, F. Ciubotaru, S. Cotofana, G. Csaba, O. V. Dobrovolskiy, C. Dubs, M. Elyasi, K. G. Fripp, H. Fulara, I. A. Golovchanskiy, C. Gonzalez-Ballestero, P. Graczyk, D. Grundler, P. Gruszecki, G. Gubbiotti, K. Guslienko, A. Haldar, S. Hamdioui, R. Hertel, B. Hillebrands, T. Hioki, A. Houshang, C.-M. Hu, H. Huebl, M. Huth, E. Iacocca, M. B. Jungfleisch, G. N. Kakazei, A. Khitun, R. Khymyn, T. Kikkawa, M. Klaui, O. Klein, J. W. Klos, S. Knauer, S. Koraltan, M. Kostylev, M. Krawczyk, I. N. Krivorotov, V. V. Kruglyak, D. Lachance-Quirion, S. Ladak, R. Lebrun, Y. Li, M. Lindner, R. MacEdo, S. Mayr, G. A. Melkov, S. Mieszczak, Y. Nakamura, H. T. Nembach, A. A. Nikitin, S. A. Nikitov, V. Novosad, J. A. Otalora, Y. Otani, A. Papp, B. Pigeau, P. Pirro, W. Porod, F. Porrati, H. Qin, B. Rana, T. Reimann, F. Riente, O. Romero-Isart, A. Ross, A. V. Sadovnikov, A. R. Safin, E. Saitoh, G. Schmidt, H. Schultheiss, K. Schultheiss, A. A. Serga, S. Sharma, J. M. Shaw, D. Suess, O. Surzhenko, K. Szulc, T. Taniguchi, M. Urbanek, K. Usami, A. B. Ustinov, T. Van Der Sar, S. Van Dijken, V. I. Vasyuchka, R. Verba, S. V. Kusminskiy, Q. Wang, M. Weides, M. Weiler, S. Wintz, S. P. Wolski, and X. Zhang, "Advances in magnetics roadmap on spin-wave computing," IEEE Trans. Magn. **58**(6), 1 (2022).

[2]B. Flebus, D. Grundler, B. Rana, Y. Otani, I. Barsukov, A. Barman, G. Gubbiotti, P. Landeros, J. Akerman, U. Ebels, P. Pirro, V. E. Demidov, K. Schultheiss, G. Csaba, Q. Wang, F. Ciubotaru, D. E. Nikonov, P. Che, R. Hertel, T. Ono, D. Afanasiev, J. Mentink, T. Rasing, B. Hillebrands, S. V. Kusminskiy, W. Zhang, C. R. Du, A. Finco, T. van der Sar, Y. K. Luo, Y. Shiota, J. Sklenar, T. Yu, and J. Rao, "The 2024 magnonics roadmap," J. Phys.: Condens. Matter **36**(36), 363501 (2024).

[3]A. V. Chumak, V. I. Vasyuchka, A. A. Serga, and B. Hillebrands, "Magnon spintronics," Nat. Phys. **11**(6), 453–461 (2015).

[4]S. Takei and Y. Tserkovnyak, "Superfluid spin transport through easy-plane ferromagnetic insulators," Phys. Rev. Lett. **112**(22), 227201 (2014).

[5]L. J. Cornelissen, J. Liu, R. A. Duine, J. Ben Youssef, and B. J. Van Wees, "Long-distance transport of magnon spin information in a magnetic insulator at room temperature," Nat. Phys. **11**(12), 1022–1026 (2015).

[6]M. C. Onbasli, A. Kehlberger, D. H. Kim, G. Jakob, M. Kläui, A. V. Chumak, B. Hillebrands, and C. A. Ross, "Pulsed laser deposition of epitaxial yttrium iron garnet films with low gilbert damping and bulk-like magnetization," APL Mater. **2**, 106102 (2014).

[7]Y. Tserkovnyak, A. Brataas, and G. E. W. Bauer, "Spin pumping and magnetization dynamics in metallic multilayers," Phys. Rev. B **66**(22), 224403 (2002).

[8]S. Yakata, Y. Ando, T. Miyazaki, and S. Mizukami, "Temperature dependences of spin-diffusion lengths of Cu and Ru layers," Jpn. J. Appl. Phys., Part 1 **45**(5 A), 3892–3895 (2006).

[9]C. Swindells, A. T. Hindmarch, A. J. Gallant, and D. Atkinson, "Spin transport across the interface in ferromagnetic/nonmagnetic systems," Phys. Rev. B **99**(6), 064406 (2019).

[10]M. B. Jungfleisch, V. Lauer, R. Neb, A. V. Chumak, and B. Hillebrands, "Improvement of the yttrium iron garnet/platinum interface for spin pumping-based applications," Appl. Phys. Lett. **103**(2), 022411 (2013).

[11]C. Hauser, T. Richter, N. Homonnay, C. Eisenschmidt, M. Qaid, H. Deniz, D. Hesse, M. Sawicki, S. G. Ebbinghaus, and G. Schmidt, "Yttrium iron garnet thin films with very low damping obtained by recrystallization of amorphous material," Sci. Rep. **6**, 20827 (2016).

[12]D. M. Cheshire, J. A. D. Nascimento, V. K. Lazarov, and S. A. Cavill, "Enhanced magnon transport through an amorphous magnetic insulator," Phys. Rev. B **109**(13), 134432 (2024).

[13]C. J. Love, B. Kuerbanjiang, A. Kerrigan, S. Yamada, K. Hamaya, G. Van Der Laan, V. K. Lazarov, and S. A. Cavill, "Substrate dependent reduction of gilbert damping in annealed Heusler alloy thin films grown on group IV semiconductors," Appl. Phys. Lett. **119**(17), 172404 (2021).

[14]Z. Celinski, K. B. Urquhart, and B. Heinrich, "Using ferromagnetic resonance to measure the magnetic moments of ultrathin films," J. Magn. Magn. Mater. **166**(1), 6–26 (1997).

[15]C. Love, J. E. Beevers, B. Achinuq, R. Fan, K. Matsuzaki, T. Susaki, V. K. Lazarov, S. S. Dhesi, G. Van Der Laan, and S. A. Cavill, "Elucidation of orbital moment, anisotropy, and magnetic damping in epitaxial Fe_3O_4 films," Phys. Rev. B **107**(6), 064414 (2023).

[16]S. S. Dhesi, S. A. Cavill, A. Potenza, H. Marchetto, R. A. Mott, P. Steadman, A. Peach, E. L. Shepherd, X. Ren, U. H. Wagner, and R. Reininger, "The nanoscience beamline (I06) at diamond light source," AIP Conf. Proc. **1234**, 311–314 (2010).

[17]R. Nakajima, J. Stöhr, and Y. U. Idzerda, "Electron-yield saturation effects in l-edge x-ray magnetic circular dichroism spectra of Fe, Co, and Ni," Phys. Rev. B **59**, 6421–6429 (1999).

[18]An additional sample, annealed at 300 °C in oxygen and capped by Pt was added to the dataset at the request of the reviewers.

[19]P. Hansen, "Anisotropy and magnetostriction of gallium-substituted yttrium iron garnet," J. Appl. Phys. **45**(8), 3638–3642 (1974).

[20]D. Cheshire, P. Bencok, D. Gianolio, G. Cibin, V. K. Lazarov, G. Van Der Laan, and S. A. Cavill, "Absence of spin-mixed states in ferrimagnet yttrium iron garnet," J. Appl. Phys. **132**(10), 103902 (2022).

[21]S. A. Manuilov, S. I. Khartsev, and A. M. Grishin, "Pulsed laser deposited $Y_3Fe_5O_{12}$ films: Nature of magnetic anisotropy I," J. Appl. Phys. **106**(12), 123917 (2009).

[22]H. Chang, P. Li, W. Zhang, T. Liu, A. Hoffmann, L. Deng, and M. Wu, "Nanometer-thick yttrium iron garnet films with extremely low damping," IEEE Magn. Lett. **5**, 1–4 (2014).
[23]D. E. Parkes, L. R. Shelford, P. Wadley, V. Holý, M. Wang, A. T. Hindmarch, G. Van Der Laan, R. P. Campion, K. W. Edmonds, S. A. Cavill, and A. W. Rushforth, "Magnetostrictive thin films for microwave spintronics," Sci. Rep. **3**, 2220 (2013).
[24]G. Schmidt, C. Hauser, P. Trempler, M. Paleschke, and E. T. Papaioannou, "Ultra thin films of yttrium iron garnet with very low damping: A review," Phys. Status Solidi B **257**(7), 1900644 (2020).
[25]M. M. Qaid, T. Richter, A. Müller, C. Hauser, C. Ballani, and G. Schmidt, "Radiation damping in ferromagnetic resonance induced by a conducting spin sink," Phys. Rev. B **96**(18), 184405 (2017).
[26]M. A. W. Schoen, J. M. Shaw, H. T. Nembach, M. Weiler, and T. J. Silva, "Radiative damping in waveguide-based ferromagnetic resonance measured via analysis of perpendicular standing spin waves in sputtered permalloy films," Phys. Rev. B **92**(18), 184417 (2015).
[27]G. van der Laan and A. I. Figueroa, "X-ray magnetic circular dichroism - A versatile tool to study magnetism," Coord. Chem. Rev. **277-278**, 95–129 (2014).
[28]B. B. Krichevtsov, S. V. Gastev, S. M. Suturin, V. V. Fedorov, A. M. Korovin, V. E. Bursian, A. G. Banshchikov, M. P. Volkov, M. Tabuchi, and N. S. Sokolov, "Magnetization reversal in YIG/GGG(111) nanoheterostructures grown by laser molecular beam epitaxy," Sci. Technol. Adv. Mater. **18**(1), 351–363 (2017).
[29]H. B. Vasili, B. Casals, R. Cichelero, F. Macià, J. Geshev, P. Gargiani, M. Valvidares, J. Herrero-Martin, E. Pellegrin, J. Fontcuberta, and G. Herranz, "Direct observation of multivalent states and $4f \rightarrow 3d$ charge transfer in Ce-doped yttrium iron garnet thin films," Phys. Rev. B **96**, 014433 (2017).
[30]R. Yu, J. Cao, H. Liu, F. Zhu, X. Meng, Z. Long, J. Li, and Y. Wang, "Pure spin transport in YIG films with amorphous-to-crystalline transformation," Adv. Phys. Res. **3**(6), 2300147 (2024).
[31]G. F. Dionne, "The magnetoelastic ion: Friend and foe to microwaves," IEEE Trans. Magn. **47**(2), 272–278 (2011).
[32]C. L. Jermain, S. V. Aradhya, N. D. Reynolds, R. A. Buhrman, J. T. Brangham, M. R. Page, P. C. Hammel, F. Y. Yang, and D. C. Ralph, "Increased low-temperature damping in yttrium iron garnet thin films," Phys. Rev. B **95**, 174411 (2017).
[33]S. Emori, D. Yi, S. Crossley, J. J. Wisser, P. P. Balakrishnan, B. Khodadadi, P. Shafer, C. Klewe, A. T. N'Diaye, B. T. Urwin, K. Mahalingam, B. M. Howe, H. Y. Hwang, E. Arenholz, and Y. Suzuki, "Ultralow damping in nanometer-thick epitaxial spinel ferrite thin films," Nano Lett. **18**(7), 4273–4278 (2018).